Electronic Supplementary Information (ESI)
This journal is (c) The Royal Society of Chemistry 2021

Photoelectrochemical immunoassay of interleukin-6 based on covalent reaction-triggered photocurrent polarity switching of ZnO@fullerenol

Min Zhou, Ying Ying, Hui Huang, Yueming Tan,* Wenfang Deng, and Qingji Xie

Key Laboratory of Chemical Biology and Traditional Chinese Medicine Research (Ministry of Education of China), College of Chemistry and Chemical Engineering, Hunan Normal University, Changsha 410081, China

*E-mail: tanyueming0813@126.com.

Experimental section

Chemicals. Fullerenol was purchased from Shanghai Rhawn Chemical Technology Co., Ltd (Shanghai, China). Chloranilic acid, and tetrabutylammonium hydroxide was purchased from Shanghai Makclin Biochemical Co., Ltd (Shanghai, China). Zinc acetate, ethanolamine, ethylene glycol, *N*-dimethyl formamide, Triton X-100, and toluene were purchased from Sinopharm Chemical Reagent Co. Ltd. (Shanghai, China). Bovine serum albumin (BSA), dipalmitoylphosphoethanolamine, dipalmitoyl phosphocholine, cholesterol, *N*-(3-(dimethylamino)propyl)-*N*-ethylcarbodiimide hydrochloride, *N*-hydroxysuccinimide, and IL-6 ELISA (Enzyme-Linked Immunosorbent Assay) kit were purchased from Sigma-Aldrich. Human serum samples were provided volunteers at The Fourth Hospital of Changsha. Carboxyl-functionalized Fe_3O_4 nanoparticles were purchased from Aladdin. All other reagents were analytical grade and without further purification. The washing and blocking buffer solution for immunoassay was 0.01 M phosphate buffer saline (PBS, pH 7.4, 0.01M NaH_2PO_4-Na_2HPO_4 + 0.15M NaCl). Milli-Q ultrapure water (Millipore, ≥18 MΩ cm) was used throughout.

Instrumentation. Transmission electron microscopy (TEM) studies were performed on a TECNAI F-30 high-resolution transmission electron microscope. Scanning electron microscopy (SEM) studies were performed on a Hitachi S4800 scanning electron microscope. Ultraviolet-visible (UV-Vis) absorption spectra were recorded on a UV2450 spectrophotometer (Shimadzu, Japan). Fourier transform infrared (FTIR) spectra were collected on Nicolet Nexus 670 Fourier transform infrared spectrometer. UV photoelectron spectroscopy (UPS) studies were performed a VG Scienta R4000 analyzer with a

monochromatic He I light source (21.2 eV), and a bias of -10 V was applied to observe the secondary electron cutoff. All photoelectrochemical experiments were carried out using a CEL-HXF300 xenon lamp light source system, and the photocurrent was recorded on a CHI760E electrochemical workstation (CH Instrument Co., Inc.) using a three-electrode system. In the three-electrode system, a photoelectrode, a saturated calomel electrode (SCE), and a platinum wire electrode served as the working electrode, the reference electrode, and counter electrode, respectively.

Synthesis of ZnO@COH microrods. ZnO microrods were synthesized following a previous report.[1] Briefly, $Zn(CH_3COO)_2 \cdot 2H_2O$ (0.44 g) was added in ethanolamine (10 mL) under magnetic stirring, followed by adding 5 mL of water and 15 mL of ethylene glycol. After sonication for 30 min, the solution was hydrothermally treated at 180 °C for 4 h. Finally, the ZnO microrods were centrifuged, washed, vacuum-dried, and grinded for future use. For the preparation of ZnO@COH microrods, 16 mg of ZnO and 1 mg of COH was mixed in 4 mL of water by sonication for 5 min.

Preparation of CA@liposome immunonanocapsules. A mixture consisting of chloroform (4 mL), dipalmitoyl phosphocholine (22 mg), cholesterol (11.6 mg), and dipalmitoyl phosphoethanolamine (3.5 mg) was ultrasonically treated for 10 min in a N_2 atmosphere. To produce a lipid film, the mixture was rotationally evaporated at 45 °C under 0.7 kPa, followed by adding 5 mL of 10 mM aqueous CA. Afterward, the lipid film was hydrated at 45 °C for 2 h and then ultrasonically treated for 10 min. The excess CA was removed by dialyzing against 10 mM PBS (pH 7.4) for 48 h. Finally, the CA@liposome nanocapsules were obtained by centrifugation and vacuum-freeze drying. To prepare CA@liposome immunonanocapsules, 1

mg of CA@liposome nanocapsules, 2 mg of *N*-hydroxysuccinimide, 4 mg of *N*-(3-(dimethylamino)propyl)-*N*-ethylcarbodiimide hydrochloride, and 100 μL of 0.1 mg mL^{-1} anti-IL-6 antibody (Ab) were mixed in 5 mL of PBS. The mixture was vigorously shaken for 4 h, and then the CA@liposome-Ab conjugates were separated by centrifugation, and resuspended in 5 mL 1 wt% bovine serum albumin aqueous solution. After shaking for 30 min, the immunonanocapsules were separated by centrifugation, washed, and freeze-dried for future use. The preparation of immunomagnetic nanobeads was similar to that in our previous study,[2] except the change in the corresponding Ab.

PEC immunoassay of IL-6. 80 μL of ZnO@COH suspension (4.25 mg mL^{-1}) was casted on a clean ITO (1.0 cm^2) to prepare a ZnO@COH/ITO photoelectrode. A certain concentration of IL-6 was incubated with 1.0 mg mL^{-1} immunonanocapsules and 0.4 mg mL^{-1} immunomagnetic nanobeads in PBS for 40 min at 37 ^oC. To release CA, the product collected after magnetic separation was lysed by 0.025 mL of 1.0 wt% Triton X-100 aqueous solution for 0.5 h. Then the ZnO@COH/ITO photoelectrode was incubated with the lysis solution under xenon lamp irradiation for 10 min. Finally, the ZnO@COH/ITO photoelectrode after the covalent reaction with CA was subjected to PEC measurements under xenon lamp irradiation (full-band wavelength light, 100 mW cm^{-2}). All PEC measurements were performed at -0.20 V (vs SCE) in 0.1 M PBS (pH 7.4).

ELISA for the detection of IL-6. In the sandwich ELISA with standard polystyrene 96-well plates, 100 μL serum sample suspension was incubated for 2.5 h at room temperature with gently shaking, and the wells were rinsed 4 times with PBS. Following that, 100 μL of 1× prepared biotinylated detection antibody was added to each well, and incubated for 60 min at

room temperature with gentle shaking. The well was washed as before. 100 μL of ELISA colorimetric TMB reagent was injected to each well, and incubated at room temperature for 30 min in the dark with gentle shaking. The enzymatic reaction was stopped by adding 100 μL of 1 M H_2SO_4 to each well. The results of ELISA were measured by a spectrophotometric ELISA reader at a wavelength of 450 nm.

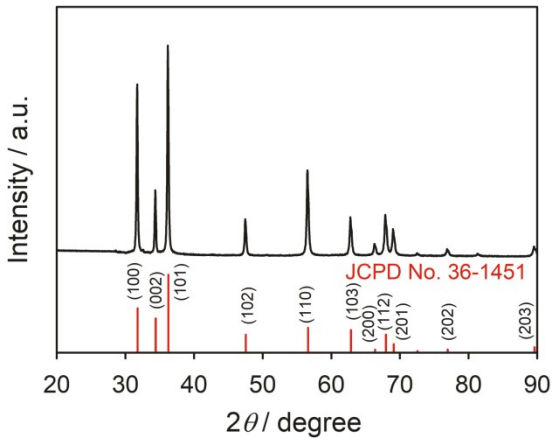

Fig. S1 XRD pattern of ZnO microrods.

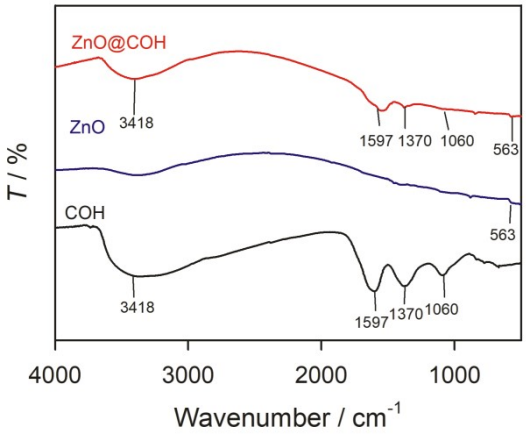

Fig. S2 FTIR spectra of COH, ZnO, and ZnO@COH.

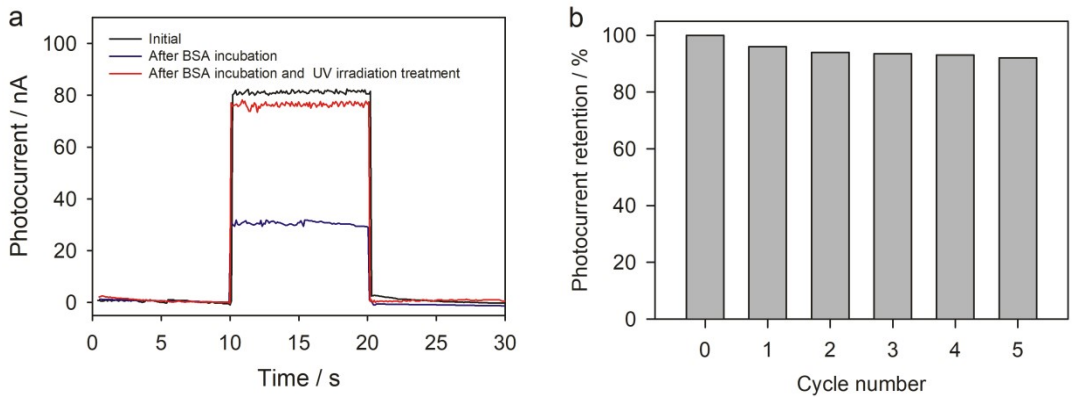

Fig. S3 (a) Photocurrent responses of ZnO@COH/ITO after BSA incubation (1 mg mL^{-1}) and UV irradiation treatment for 5 min. (b) Photocurrent retention of ZnO@COH/ITO after BSA adsorption and UV irradiation treatment for different cycles. PEC measurements were performed at -0.20 V (vs SCE) in 0.1 M PBS (pH 7.4).

As shown in **Fig. S3a**, the photocurrent response of ZnO@COH/ITO after BSA incubation (1 mg mL^{-1}) decreases seriously, due to the adsorption of BSA on ZnO@COH/ITO. Interestingly, the photocurrent response of ZnO@COH/ITO can be recovered after UV irradiation treatment for 5 min, indicating that the ZnO@COH/ITO has excellent photocatalytic self-cleaning ability. Moreover, the ZnO@COH/ITO can still retain 91% of its initial photocurrent response after BSA adsorption and UV irradiation treatment for 5 cycles (**Fig. S3b**). The excellent photocatalytic self-cleaning ability enables the reusability of the photoelectrode.

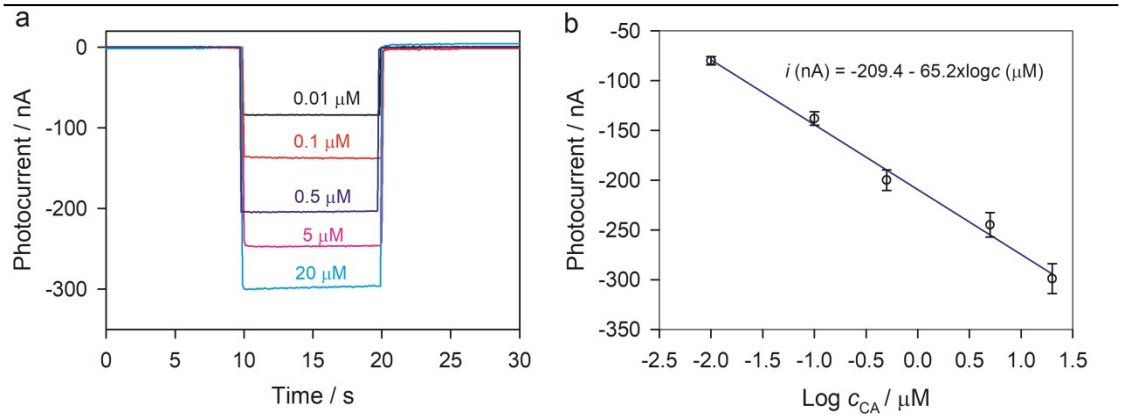

Fig. S4 (a) Photocurrent responses of ZnO@COH/ITO after covalent reaction with different concentrations of CA. (b) Photocurrent as a function of CA concentration.

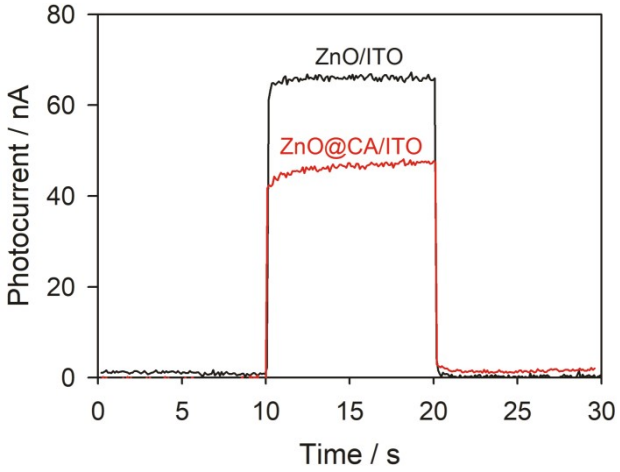

Fig. S5 Photocurrent responses of ZnO/ITO and ZnO@CA/ITO at -0.20 V vs SCE in 0.1 M PBS (pH 7.4).

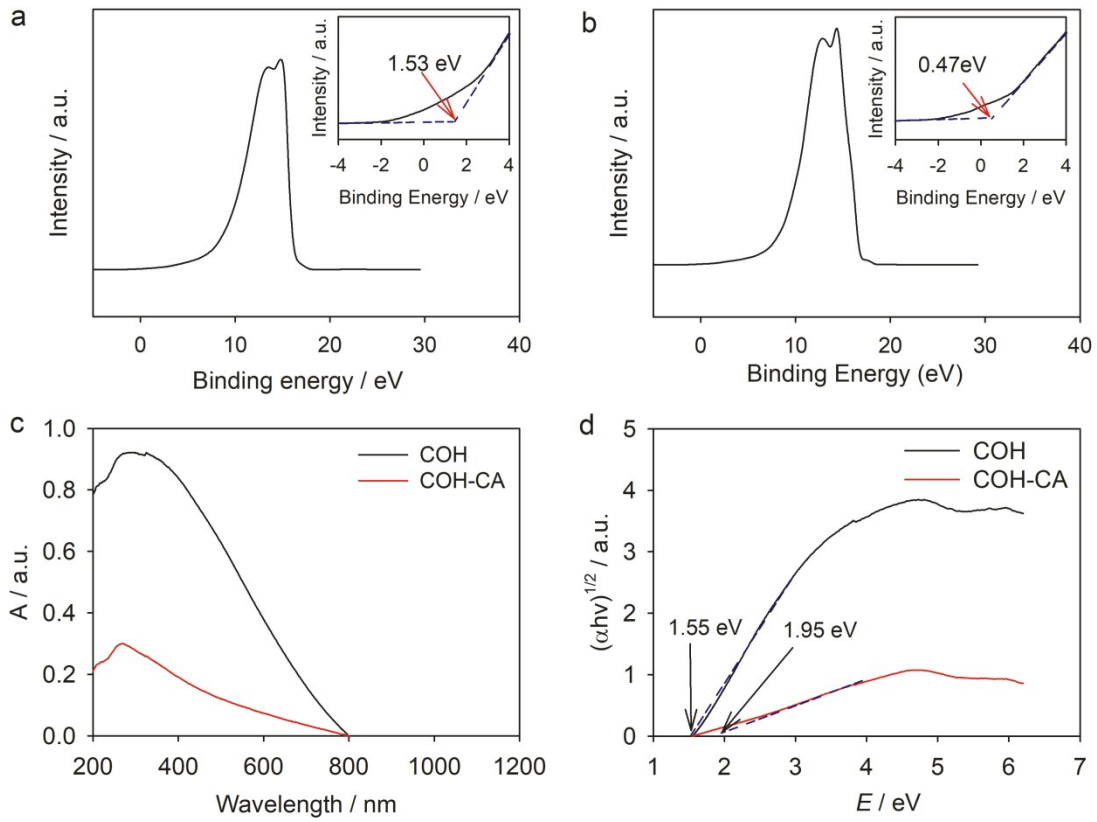

Fig. S6 UV photoelectron spectra of (a) COH and (b) COH-CA. Inset shows hole injection barriers of (a) COH and (b) COH-CA. (c) UV-Vis diffuse reflection spectra and (d) band gap profiles of COH and COH-CA.

To understand the mechanism for the covalent reaction-triggered photocurrent polarity switch of ZnO@COH, UV photoelectron spectroscopy (UPS) and UV-Vis diffuse reflection spectroscopy were carried out to measure the energy-level positions of COH and COH-CA (reaction product of 20 mg mL^{-1} COH and 5 mg mL^{-1} CA under xenon lamp irradiation for 10 min). Based on UV photoelectron spectra data (**Fig. S6a** and **b**), the Fermi levels of COH and COH-CA obtained from the Avantage software are -0.57 and -0.14 eV, respectively. The hole injection barriers (the energy difference between Fermi level and the highest occupied molecular orbital (HOMO)) of COH and COH-CA can be estimated to be 1.53 and 0.47 eV,

respectively (inset of **Fig. S6a** and **b**). Thus the HOMO of COH and COH-CA can be estimated to be 0.96 and 0.33 eV, respectively. To obtain the band gaps (E_g) of COH and COH-CA, UV-Vis diffuse reflection spectroscopy was carried out (**Fig. S6c**). The value of E_g is estimated according to the equation of $\alpha h\nu = A(h\nu - E_g)^{n/2}$, where α is the absorption coefficient, h is the Planck constant, ν is the frequency of light, A is a constant, and n is 1 for organic materials.[3] Thus value of E_g can be estimated from the tangent intercept (**Fig. S6d**). The value of E_g for COH and COH-CA are estimated to be 1.55 and 1.95 eV, respectively. According to the equation $E_{LUMO}=E_{HOMO}-E_g$, the lowest unoccupied molecular orbitals (LUMO) are calculated to be -0.59 and -1.62 eV, respectively.

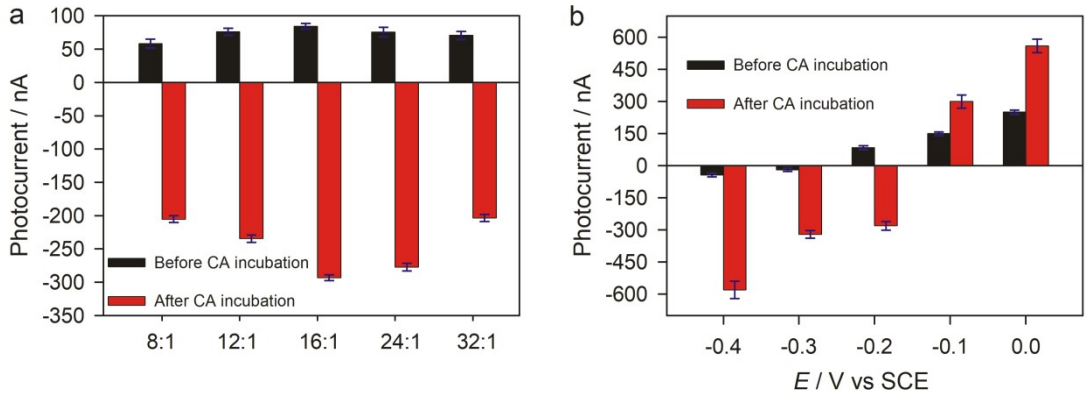

Fig. S7 Effects of (a) ZnO/COH weight ratio and (b) bias potential on the photocurrent response of ZnO@COH/ITO.

The weight ratio between ZnO and COH plays an important role in the photocurrent response of ZnO@COH/ITO (**Fig. S7a**). At a ZnO/COH ratio of 16:1, the as-prepared ZnO@COH/ITO exhibits the highest anodic photocurrent before CA incubation and the highest cathodic photocurrent after CA incubation. Thus ZnO@COH with a ZnO/COH ratio of 16:1 was used to prepare ZnO@COH/ITO for PEC immunoassay in this work. As is well known, the bias potential can affect the photocurrent polarity,[4] so the bias potential was optimized (**Fig. S7b**). Before CA incubation, the ZnO@COH/ITO exhibits anodic photocurrents at potentials higher than -0.2 V (vs SCE); after CA incubation, the ZnO@COH/ITO exhibits cathodic photocurrents at potentials lower than -0.2 V. At a bias potential of -0.2 V, the photocurrent polarity of ZnO@COH/ITO can be switched by CA incubation, so -0.2 V is chosen for PEC immunoassay in this work.

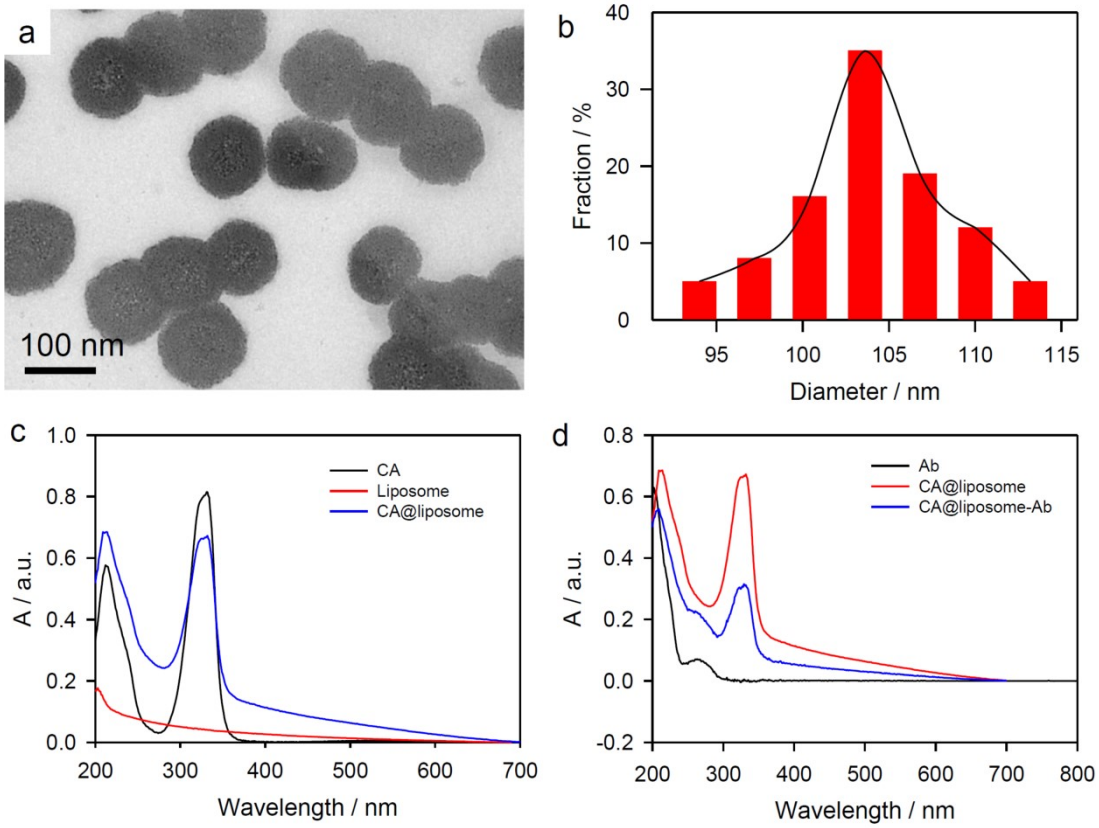

Fig. S8 (a) TEM image and (b) size distribution of CA@liposome. (c) UV−vis spectra of CA, liposome, and CA@liposome. (d) UV−vis spectra of Ab, CA@liposome, and CA@liposome-Ab.

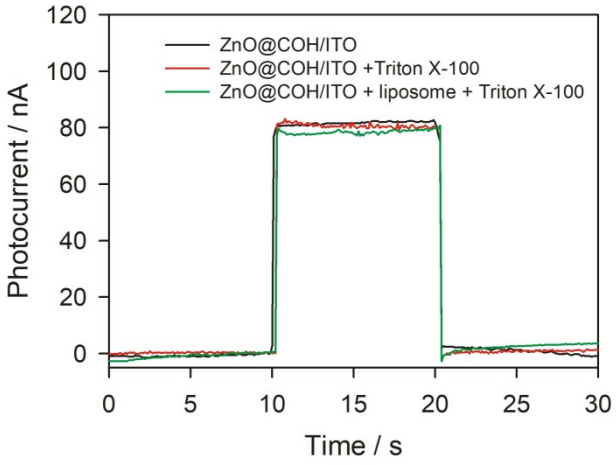

Fig. S9 Photocurrent responses of ZnO@COH/ITO after the incubation with Triton X-100 (1 wt%) and liposome (1 mg mL^{-1}). PEC measurements were performed at -0.20 V (vs SCE) in 0.1 M PBS (pH 7.4).

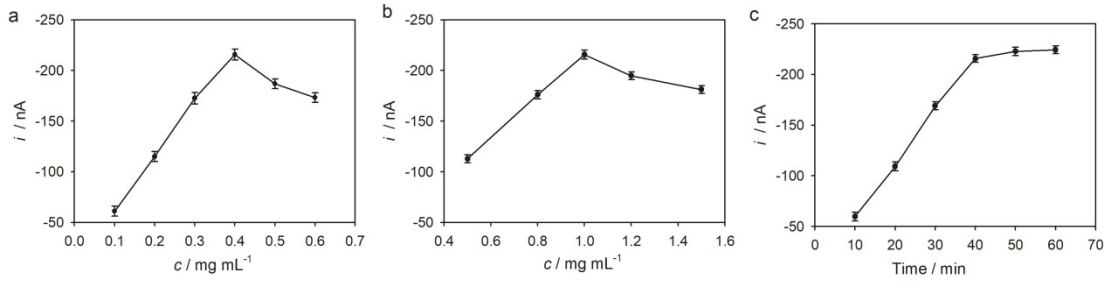

Fig. S10 Effects of (a) concentration of immunomagnetic nanobeads, (b) concentration of CA@liposome immunonanocapsules, and (c) incubation time on photocurrent responses for detecting 10 pg mL^{-1} IL-6.

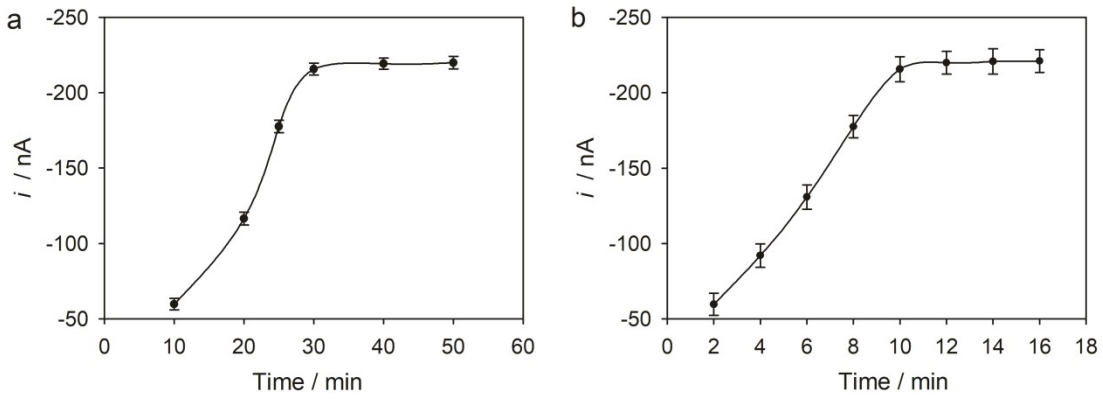

Fig. S11 Effects of (a) CA release time and (b) covalent reaction time on photocurrent responses for detecting 10 pg mL^{-1} IL-6.

Table S1. Performance Comparison of IL-6 Detection in the Literature.

Technique	Linear range (ng mL^{-1})	Detection limit (ng mL^{-1})	Ref.
Electrochemical	1×10^{-5}-2×10^{-3}	3×10^{-6}	5
Electrochemical	1×10^{-3}-10	1×10^{-3}	6
Electrochemical	2.5×10^{-5}-10	7×10^{-6}	7
Fluorescence	4×10^{-4}-0.4	1×10^{-4}	8
Fluorescence	2×10^{-3}-2.4	2×10^{-3}	9
Photoluminescence	2×10^{-2}-20	8×10^{-3}	10
Photoelectrochemical	5×10^{-6}-1	2×10^{-6}	11
Photoelectrochemical	5×10^{-5}-10	2×10^{-5}	12
Photoelectrochemical	1×10^{-3}-1×10^{2}	3.8×10^{-4}	13
Photoelectrochemical	5×10^{-6}-10	1×10^{-6}	This work

Table S2. Analysis results for determination of IL-6 in human serum samples.

Sample	Proposed Method					ELISA				
	Original (pg mL^{-1})	Spiked (pg mL^{-1})	Found (pg mL^{-1})	Recovery (%)	RSD (%)	Original (pg mL^{-1})	Spiked (pg mL^{-1})	Found (pg mL^{-1})	Recovery (%)	RSD (%)
		5.0	9.27	98.4	4.9		5.0	9.68	103	4.7
#1	4.39	10.0	15.1	105	6.2	4.42	10.0	14.2	98.5	3.9
		15.0	20.2	104	5.8		15.0	19.0	97.8	4.3
		10.0	20.1	104	5.3		10.0	18.9	97.9	4.1
#2	9.37	20.0	30.3	103	4.4	9.31	20.0	28.9	98.6	3.5
		30.0	38.7	98.4	4.5		30.0	40.2	102	3.3

References:

1 C. J. Jing, Z. Y. Pan, H. Y. Zou, Y. F. Li, P. F. Gao and C. Z. Huang, *Anal. Chim. Acta* 2020, **1109**, 107-113.

2 L. Yang, W. Deng, C. Cheng, Y. Tan, Q. Xie and S. Yao, *ACS Appl. Mater. Interfaces* 2018, **10**, 3441-3448.

3 X. Y. Zhang, L. Han, L. Dan Yu, X. H. Wang, Y. Ling, N. B. Li and H. Q. Luo, *ACS Appl. Mater. Interfaces* 2021, **13**, 15881-15889.

4 X. Zhong, M. Zhang, L. a. Guo, Y. Xie, R. Luo, W. Chen, F. Cheng and L. Wang, *Biosens. Bioelectron.* 2021, **189**, 113389-113389.

5 N. Ozcan, C. Karaman, N. Atar, O. Karaman and M. L. Yola, *ECS J. Solid State Sci. Technol.* 2020, **9**, 121010.

6 F. Khosravi, S. M. Loeian and B. Panchapakesan, *Biosensors* 2017, **7**, 13.

7 L. Cao, J. Cai, W. Deng, Y. Tan and Q. Xie, *Anal. Chem.* 2020, **92**, 16267-16273.

8 K. Zhang, G. Liu and E. M. Goldys, *Biosens. Bioelectron.* 2018, **102**, 80-86.

9 M. Toma and K. Tawa, *Biosens. Bioelectron.* 2016, **8**, 22032-22038.

10 W. W. Xiong, G. H. Yang, X. C. Wu and J. J. Zhu, *ACS Appl. Mater. Interfaces* 2013, **5**, 8210-8216.

11 R. D. Crapnell, W. Jesadabundit, A. G.-M. Ferrari, N. C. Dempsey-Hibbert, M. Peeters, A. Tridente, O. Chailapakul and C. E. Banks, *Anal. Chem.* 2021, **93**, 5931–5938.

12 B. Ran, Y. Xianyu, M. Dong, Y. Chen, Z. Qian and X. Jiang, *Anal. Chem.* 2017, **89**, 6113–6119.

13 L. Gong, H. Dai, S. Zhang and Y. Lin, *Anal. Chem.* 2016, **88**, 5775–5782.